

Next-Generation Grid Codes: Toward a New Paradigm for Dynamic Ancillary Services

Verena Häberle[†], Kehao Zhuang[§], Xiuqiang He[‡], Linbin Huang[§], Gabriela Hug[†], Florian Dörfler[†]

Abstract—This paper presents *preliminary results* toward a conceptual foundation for *Next Generation Grid Codes (NGGCs)* based on decentralized stability and performance certification for dynamic ancillary services. The proposed NGGC framework targets two core outcomes: (i) guaranteed closed-loop stability and (ii) explicit performance assurances for power-system frequency and voltage dynamics. Stability is addressed using loop-shifting and passivity-based methods that yield local frequency-domain certificates for individual devices, enabling fully decentralized verification of the interconnected system. Performance is characterized by deriving quantitative bounds on key time-domain metrics (e.g., nadirs, rate-of-change-of-frequency (RoCoF), steady-state deviations, and oscillation damping) through frequency-domain constraints on local device behavior. The framework is non-parametric and model-agnostic, accommodating a broad class of device dynamics under mild assumptions, and provides an initial unified approach to stability and performance certification without explicit device-model parameterization. As such, these results offer a principled starting point for the development of future grid codes and control design methodologies in modern power systems.

I. INTRODUCTION

Current grid codes for dynamic ancillary services provision with converter-based generation, such as fast frequency and voltage regulation, are predominantly specified through prescribed time-domain step responses and response-time limits. The European network code [1], for instance, defines frequency containment and voltage regulation via piecewise-linear active and reactive power curves. National codes in Finland [2] and Germany [3] similarly prescribe fast frequency reserves and synthetic inertia using power injection profiles or time constants. Although conceptually simple, these requirements are often implemented via open-loop commands or look-up tables, resulting in rigid and inefficient control. Moreover, existing codes focus mainly on grid-following operation, with only recent exceptions of including grid-forming requirements [3], and they offer no guarantees of closed-loop stability or system performance. As a result, systems that comply with current grid codes may still exhibit poor dynamic behavior or instability [4], [5].

Recent grid-code proposals [6] have begun to address closed-loop stability and performance guarantees using frequency-domain concepts. However, their scope remains limited to single-device-to-grid connections and qualitative disturbance rejection, without providing explicit bounds on key metrics such as frequency nadir or RoCoF. Related efforts to incorporate passivity requirements into grid-forming control design [7] face similar challenges, as power system networks are not inherently passive. These limitations motivate the formulation of a more

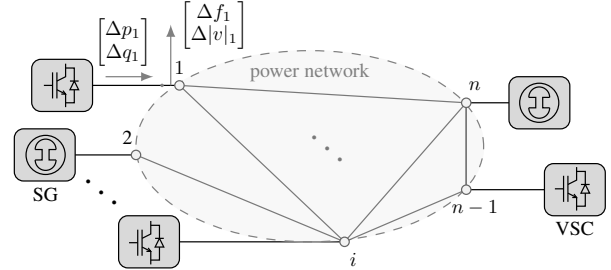


Fig. 1: Multi-device transmission system with SGs and grid-forming VSCs connected by resistive-inductive transmission lines.

general, quantitative, and practically implementable framework to specify dynamic ancillary services in future grid codes.

This paper introduces the concept of *Next Generation Grid Codes (NGGCs)* as a first step toward a new paradigm for dynamic ancillary services provision based on decentralized frequency-domain criteria. The NGGC framework provides two main benefits: (i) guaranteed closed-loop stability and (ii) explicit performance guarantees at the system level. For stability, we employ loop-shifting and passivity-based techniques to derive decentralized certificates that translate into local tuning rules for individual devices, ensuring modular contributions to global stability. For performance, we establish quantitative bounds on critical time-domain indicators of small-signal frequency and voltage dynamics, including frequency and voltage nadirs, RoCoF, steady-state deviations, and oscillation damping. These bounds are obtained by linking time-domain metrics to frequency-domain constraints on local device behavior and can be expressed as Nyquist-plot envelopes on device transfer functions. The framework naturally accommodates grid-forming signal causality and integrates with existing converter and synchronous-generator models.

Unlike existing decentralized stability certification methods that rely on explicit device parameterizations [4], [8], [9], the proposed approach is model-agnostic and applies to heterogeneous devices under mild behavioral assumptions. While related generic certificates based on small-gain, small-phase, or sector conditions have been reported [10], [11], the present work extends these results by simultaneously providing explicit stability and performance guarantees. To the best of our knowledge, this is the first unified framework that ensures both closed-loop stability and quantitative performance bounds for frequency and voltage dynamics under general, non-parametric device models.

II. POWER SYSTEM MODEL

Small-Signal Network Dynamics: We consider an interconnected power system composed of three-phase generation units, including grid-forming voltage-source converters (VSCs) and synchronous generators (SGs), connected through a balanced resistive-inductive transmission network. The network is rep-

[†] Verena Häberle, Gabriela Hug, and Florian Dörfler are with the Department of Electrical Engineering, ETH Zurich, 8092 Zurich, Switzerland. Email: {verenah, hug, dorfler}@ethz.ch

[§] Kehao Zhuang and Linbin Huang are with the College of Electrical Engineering, Zhejiang University, Hangzhou 310027, China. Email: {hlinbin, zhuangkh}@zju.edu.cn

[‡] Xiuqiang He is with the Department of Automation, Tsinghua University, Beijing 100084, China. Email: hxq19@tsinghua.org.cn

resented in Kron-reduced form with n generator buses, as illustrated in Fig. 1.

The network dynamics are modeled using a quasi-stationary small-signal representation in the global per-unit system, which relates deviations in bus frequencies $\Delta f = [\Delta f_1 \dots \Delta f_n]^\top$ and voltage magnitudes $\Delta|v| = [\Delta|v|_1 \dots \Delta|v|_n]^\top$ to the corresponding active and reactive power injections $\Delta p = [\Delta p_1 \dots \Delta p_n]^\top$ and $\Delta q = [\Delta q_1 \dots \Delta q_n]^\top$. Specifically, the transmission network is described by a $2n \times 2n$ transfer matrix $N(s)$ (see [9] for a detailed derivation), such that

$$\begin{bmatrix} \Delta p(s) \\ \Delta q(s) \end{bmatrix} = \underbrace{\begin{bmatrix} N^{\text{fp}}(s) & 0 \\ 0 & N^{\text{vq}} \end{bmatrix}}_{=: N(s)} \begin{bmatrix} \Delta f(s) \\ \Delta|v|(s) \end{bmatrix}, \quad (1)$$

revealing a decoupling between the active-power-frequency (pf) and reactive-power-voltage (qv) dynamics. The pf-coupling is captured by the $n \times n$ matrix $N^{\text{fp}}(s)$ with entries

$$\begin{aligned} N_{ii}^{\text{fp}}(s) &= \frac{1}{s} \frac{2\pi}{1+\rho^2} \sum_{j \neq i}^n b_{ij} |v|_{0,i} |v|_{0,j}, \\ N_{ij}^{\text{fp}}(s) &= -\frac{1}{s} \frac{2\pi}{1+\rho^2} b_{ij} |v|_{0,i} |v|_{0,j}, \end{aligned} \quad (2)$$

while the qv-coupling is described by the static $n \times n$ matrix N^{vq} with elements

$$\begin{aligned} N_{ii}^{\text{vq}} &= \frac{1}{1+\rho^2} \sum_{j \neq i}^n b_{ij} (2|v|_{0,i} - |v|_{0,j}), \\ N_{ij}^{\text{vq}} &= -\frac{1}{1+\rho^2} b_{ij} |v|_{0,i}. \end{aligned} \quad (3)$$

Here, $|v|_{0,i}$ denotes the steady-state voltage magnitude at node i , $b_{ij} = 1/l_{ij}$ is the line susceptance, and $\rho_{ij} = r_{ij}/l_{ij}$ is the resistance-to-inductance ratio of line ij . The network is assumed to be dominantly inductive, with a small and uniform $\rho_{ij} = \rho \ll 1$. If no line connects nodes i and j , we set $b_{ij} = \rho_{ij} = 0$.

Small-Signal Device Dynamics: We model generation units with grid-forming signal causality, i.e., devices that regulate frequency and voltage outputs based on measured active and reactive power deviations. The linearized dynamics of the i -th device are described by a diagonal 2×2 transfer matrix

$$- \begin{bmatrix} \Delta f_i(s) \\ \Delta|v|_i(s) \end{bmatrix} = \begin{bmatrix} D_i^{\text{pf}}(s) & 0 \\ 0 & D_i^{\text{qv}}(s) \end{bmatrix} \begin{bmatrix} \Delta p_i(s) \\ \Delta q_i(s) \end{bmatrix}. \quad (4)$$

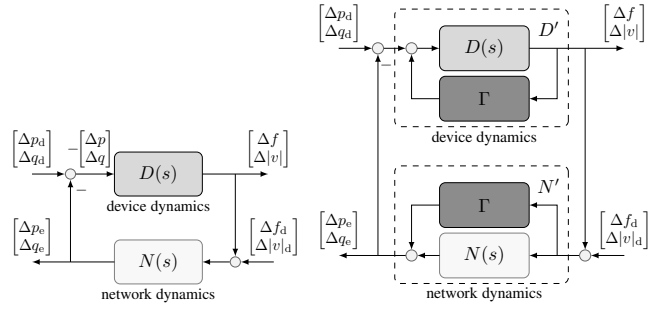
The device dynamics $D_i^{\text{pf}}(s)$ and $D_i^{\text{qv}}(s)$ allow for arbitrary rational transfer functions that capture decoupled pf- and qv-behavior. This model-agnostic representation accommodates a wide range of devices, including grid-forming VSCs and SGs, without relying on explicit parameterizations. Stacking all device models yields the overall device dynamics, i.e.,

$$- \begin{bmatrix} \Delta f(s) \\ \Delta|v|(s) \end{bmatrix} = \underbrace{\begin{bmatrix} D^{\text{pf}}(s) & 0 \\ 0 & D^{\text{qv}}(s) \end{bmatrix}}_{=: D(s)} \begin{bmatrix} \Delta p(s) \\ \Delta q(s) \end{bmatrix} \quad (5)$$

where $D^{\text{pf}}(s) = \text{diag}(D_i^{\text{pf}}(s))$ and $D^{\text{qv}}(s) = \text{diag}(D_i^{\text{qv}}(s))$.

Interconnected Power System: The closed-loop power system is modeled as the feedback interconnection of the device dynamics (5) and the network dynamics (1), denoted by $D \# N$ (Fig. 2a). Due to the decoupling of device and network dynamics, this interconnection separates into pf- and qv-subsystems.

For stability analysis, we retain the full multi-node feedback interconnection to capture inter-node coupling. For performance analysis, we adopt reduced representations consistent with grid-code practice, namely the average-mode system frequency



(a) Original feedback system. (b) Loop-shifted system with Γ .
Fig. 2: Closed-loop power system with active and reactive power disturbances Δp_d and Δq_d , and frequency and voltage disturbances Δf_d and $\Delta|v|_d$.

response of the pf-subsystem, and local voltage responses of the qv-subsystem. This enables the derivation of decentralized conditions on each $D_i^{\text{pf}}(s)$ and $D_i^{\text{qv}}(s)$, ensuring both closed-loop stability and performance of the overall power system.

Average-Mode System Frequency: Assuming stability of the pf-subsystem, the closed-loop mapping from active-power disturbances to frequency deviations is characterized by the network Laplacian. Its eigenvalue decomposition reveals that the dominant low-frequency behavior is governed by the coherent (average-mode) system frequency response [12], i.e.,

$$\Delta f_{\text{avg}}(s) \approx \underbrace{\left(\sum_{i=1}^n \left(D_i^{\text{pf}}(s) \right)^{-1} \right)^{-1}}_{=: D_{\text{avg}}(s)} \underbrace{\sum_{i=1}^n \Delta p_{d,i}(s)}_{=: \Delta p_d^{\sum}(s)}. \quad (6)$$

III. DEVICE-LEVEL CERTIFICATION METHODS

A. Stability Certification Criteria

By applying loop-shifting and passivity-based arguments as in [9], we derive decentralized device-level conditions that ensure internal feedback stability of the closed-loop interconnection $D \# N$. In particular, since the network transfer matrix $N(s)$ is not inherently passive, we introduce a block-diagonal loop-shifting matrix $\Gamma = \text{diag}(0_{n \times n}, \Gamma^{\text{qv}})$, leading to the loop-shifted interconnection $D' \# N'$ in Fig. 2b. The $n \times n$ matrix

$$\Gamma^{\text{qv}} = \text{diag}(c_i), \quad c_i = \sum_{j \neq i}^n b_{ij} \frac{0.8}{1+\rho^2}, \quad (7)$$

is selected such that the loop-shifted network $N'(s)$ is passive [9]. The corresponding loop-shifted device dynamics $D'(s)$ are

$$D'(s) = \begin{bmatrix} D^{\text{pf}}(s) & 0 \\ 0 & D^{\text{qv}}(s)(I - \Gamma^{\text{qv}} D^{\text{qv}}(s))^{-1} \end{bmatrix}. \quad (8)$$

Internal stability of $D' \# N'$ (and hence $D \# N$) follows if $D'(s)$ is strictly passive and a mild small-gain condition at $\omega = \infty$ holds [9]. Because (8) is diagonal, the conditions separate into independent constraints for the pf- and qv-channels.

Frequency control: Strict passivity and the small-gain condition of $D^{\text{pf}}(s)$ reduce, for each device i , to

$$D_i^{\text{pf}}(s) \text{ is stable and strictly proper,} \quad (1-i)$$

$$\text{Re}[D_i^{\text{pf}}(j\omega)] > 0, \quad \forall, \omega \in [0, \infty). \quad (1-ii)$$

Voltage control: Strict passivity and the small-gain condition of the loop-shifted qv-dynamics $D^{\text{qv}}(s)(I - \Gamma^{\text{qv}} D^{\text{qv}}(s))^{-1}$ are guaranteed if each device i satisfies

$$D_i^{\text{qv}}(s) \text{ is stable and strictly proper,} \quad (2-i)$$

$$\text{Re}[D_i^{\text{qv}}(j\omega)^{-1}] < 0, \quad \forall, \omega \in [0, \infty). \quad (2-ii)$$

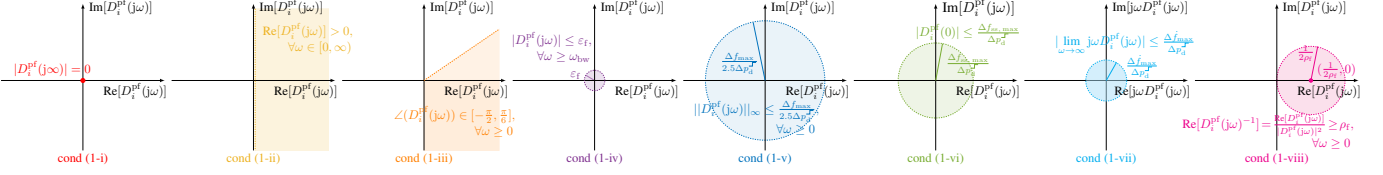


Fig. 3: Qualitative graphical illustration of the eight frequency-domain conditions (1-i) to (1-viii) for each $D_i^{\text{pf}}(j\omega)$ in the complex plane.

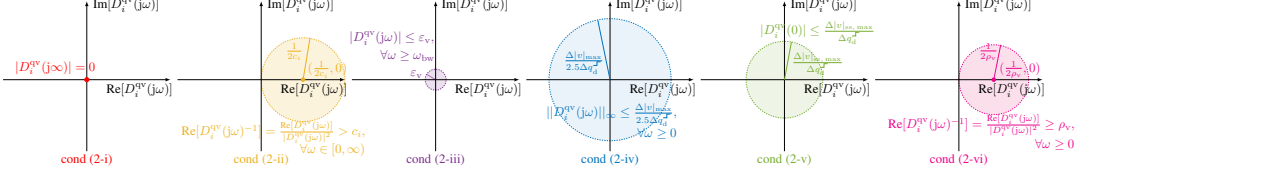


Fig. 4: Qualitative graphical illustration of the six frequency-domain conditions (2-i) to (2-vi) for each $D_i^{\text{qv}}(j\omega)$ in the complex plane.

If all devices satisfy conditions (1-i), (1-ii), (2-i), and (2-ii), then the overall interconnection $D \# N$ is internally stable.

B. Performance Certification Criteria

Frequency Control: Performance limits are imposed on the average-mode frequency response in (6) expressed through time-domain metrics after a worst-case active-power step disturbance $\Delta p_d^{\sum}(s) = \frac{1}{s}\Delta p_d^{\text{f}}$. The considered time-domain metrics include a bounded nadir $\sup_{t \geq 0} |\Delta f_{\text{avg}}^{\text{f}}(t)| \leq \Delta f_{\text{max}}$, a bounded steady-state deviation $|\lim_{t \rightarrow \infty} \Delta f_{\text{avg}}^{\text{f}}(t)| \leq \Delta f_{\text{ss,max}}$, a bounded RoCoF $\sup_{t \geq 0} |\Delta \dot{f}_{\text{avg}}^{\text{f}}(t)| \leq \Delta \dot{f}_{\text{max}}$, and sufficiently damped oscillations of $\Delta f_{\text{avg}}^{\text{f}}(t)$. These time-domain metrics are derived through a technically involved analysis exploiting properties of the Fourier integral and related algebraic arguments taken from [13]. Specifically, it can be shown that suitable decentralized constraints on each $D_i^{\text{pf}}(s)$ enforce corresponding structural properties of the aggregate transfer function $D_{\text{avg}}(s)$, which in turn imply the time-domain metrics on $\Delta f_{\text{avg}}^{\text{f}}(t)$. The full proof is omitted due to space limitations; instead, the resulting local conditions are summarized below. In particular, the *performance objectives* for $\Delta f_{\text{avg}}^{\text{f}}(t)$ are ensured if each device satisfies (1-i) and (1-ii), together with:

$$\angle(D_i^{\text{pf}}(j\omega)) \in [-\frac{\pi}{2}, \frac{\pi}{6}], \quad \forall \omega \geq 0, \quad (1-\text{iii})$$

$$|D_i^{\text{pf}}(j\omega)| \leq \varepsilon_f, \quad \forall \omega \geq \omega_{\text{bw}}, \quad (1-\text{iv})$$

$$||D_i^{\text{pf}}(j\omega)||_{\infty} \leq \frac{\Delta f_{\text{max}}}{2.5\Delta p_d^{\text{f}}}, \quad \forall \omega \geq 0, \quad (1-\text{v})$$

$$|D_i^{\text{pf}}(0)| \leq \frac{\Delta f_{\text{ss,max}}}{\Delta p_d^{\text{f}}}, \quad (1-\text{vi})$$

$$|\lim_{\omega \rightarrow \infty} j\omega D_i^{\text{pf}}(j\omega)| \leq \frac{\Delta f_{\text{max}}}{\Delta p_d^{\text{f}}}, \quad (1-\text{vii})$$

$$\text{Re}[D_i^{\text{pf}}(j\omega)^{-1}] \geq \rho_f, \quad \forall \omega \geq 0. \quad (1-\text{viii})$$

Here, ω_{bw} is a prescribed bandwidth, $\varepsilon_f \approx 0$ enforces roll-off for $\omega \geq \omega_{\text{bw}}$, and $\rho_f > 0$ is an output feedback passivity index selected to ensure adequate damping. Conditions (1-iii), (1-iv) and (1-v) bound the nadir, (1-vi) bounds the steady-state deviation, (1-vii) bounds RoCoF, and (1-viii) enforces oscillation damping. A graphical illustration of the frequency-domain conditions (1-i) to (1-viii) is provided in Fig. 3.

Voltage Control: In the qv-subsystem there is no meaningful average mode; instead, voltage deviations are predominantly local. Accordingly, we approximate

$$\Delta|v|_i(s) \approx D_i^{\text{qv}}(s)\Delta q_{d,i}(s), \quad (9)$$

and impose local time-domain bounds on the peak and steady-state voltage deviations, i.e., $\sup_{t \geq 0} |\Delta|v|_i^{\text{f}}(t)| \leq \Delta|v|_{\text{max}}$

and $|\lim_{t \rightarrow \infty} \Delta|v|_i^{\text{f}}(t)| \leq \Delta|v|_{\text{ss,max}}$, together with sufficient damping, under a worst-case reactive-power step $\Delta q_{d,i}(s) = \frac{1}{s}\Delta q_d^{\text{f}}$. These time-domain bounds are guaranteed if each device satisfies the conditions in (2-i) and (2-ii) and:

$$|D_i^{\text{qv}}(j\omega)| \leq \varepsilon_v, \quad \forall \omega \geq \omega_{\text{bw}}, \quad (2-\text{iii})$$

$$||D_i^{\text{qv}}(j\omega)||_{\infty} \leq \frac{\Delta|v|_{\text{max}}}{2.5\Delta q_d^{\text{f}}}, \quad \forall \omega \geq 0, \quad (2-\text{iv})$$

$$|D_i^{\text{qv}}(0)| \leq \frac{\Delta|v|_{\text{ss,max}}}{\Delta q_d^{\text{f}}}, \quad (2-\text{v})$$

$$\text{Re}[D_i^{\text{qv}}(j\omega)^{-1}] \geq \rho_v, \quad \forall \omega \geq 0. \quad (2-\text{vi})$$

Here, $\varepsilon_v \approx 0$ enforces roll-off beyond ω_{bw} , and $\rho_v > 0$ is chosen to ensure adequate damping. A graphical illustration of conditions (2-i) to (2-vi) is provided in Fig. 4. The proof parallels the frequency case, but applies directly to $D_i^{\text{qv}}(s)$.

IV. NEXT GENERATION GRID CODE SPECIFICATIONS

Based on the derived stability and performance conditions, we formulate *Next Generation Grid Code (NGGC)* specifications for frequency and voltage regulation: Each generation unit shall implement its pf- and qv-control via transfer functions $D_i^{\text{pf}}(s)$ and $D_i^{\text{qv}}(s)$ that satisfy the decentralized conditions in (1-i) to (1-viii) and (2-i) to (2-vi), respectively. Compliance with these specifications guarantees closed-loop stability and system-wide performance. The NGGC requirements admit an intuitive graphical interpretation in the complex plane, exemplarily illustrated by the Nyquist-pilot envelopes in Fig. 5 for the pf-control (with an analogous interpretation for the qv-control).

V. NUMERICAL EXPERIMENT

To validate the proposed NGGC framework and its stability and performance guarantees, we conduct numerical experiments in MATLAB/Simulink using a simple two-node system with two devices interconnected by an RL line. The setup follows the modeling assumptions of the NGGC framework: a quasi-stationary phasor-based network model is used, and only outer-loop device dynamics are implemented, neglecting inner converter loops and fast synchronous-machine dynamics. The numerical studies evaluate established generation-unit controls, including grid-forming VSCs and synchronous generators (SGs), with respect to the proposed NGGC conditions. We focus on the pf-subsystem while fixing all bus voltages at 1 p.u.

In the *first experiment*, one node uses a VSC with feasible control $D_1^{\text{pf}}(s)$ (satisfying conditions (1-i)–(1-viii)), while the device under test (DUT) at the second node is varied. The DUTs include static droop (DUT 1), virtual oscillator control

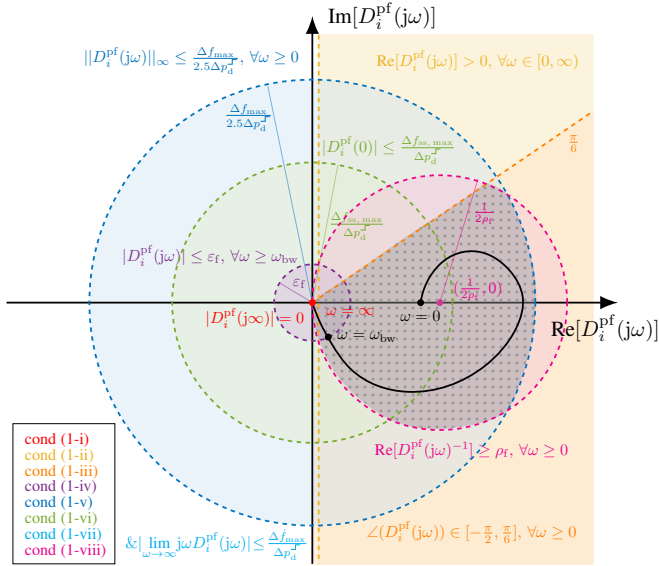


Fig. 5: Superposition of NGGC conditions (1-i) to (1-viii) in Fig. 3. The gray shaded region indicates the feasible set for all $\omega \in (0, \omega_{bw})$, and the black curve depicts an exemplary feasible Nyquist plot of $D_i^pf(j\omega)$.

(VOC) (DUT 2), virtual synchronous machine (VSM) (DUT 3), generalized second-order droop control (DUT 4), and SGs with non-reheat steam (DUT 5), reheat steam (DUT 6), and hydro turbines (DUT 7) (parameters from [14]). Their Nyquist characteristics and NGGC compliance are summarized in Fig. 6 and Table I. A 0.1 p.u. active-power step disturbance is applied at the DUT node, and the resulting average-mode frequency responses are shown in Fig. 7a. All configurations remain stable, consistent with approximate satisfaction of the strict passivity conditions (1-i) and (1-ii). While the steady-state frequency deviation remains within the ENTSO-E limit $\Delta f_{ss,max} = 0.2$ Hz for all DUTs (condition (1-vi) satisfied), the frequency nadir correlates strongly with $\|D_2^pf(s)\|_\infty$. Although SG-based DUTs 5-7 violate condition (1-v), the ideal VSC at node 1 limits the nadir well below the ENTSO-E bound $\Delta f_{max} = 0.8-1$ Hz. RoCoF behavior and oscillation damping are consistent with conditions (1-vii) and (1-viii), respectively, where DUT 1&2 and DUT 4, violating condition (1-vii), exhibit the highest RoCoF values, even exceeding the ENTSO-E limit of $\Delta f_{max} = 2$ Hz/s.

In the *second experiment*, both nodes are equipped with identical DUTs. The corresponding frequency responses in Fig. 7b exhibit markedly degraded performance: the nadir exceeds the ENTSO-E limit for DUT 7 (violation of conditions (1-iii) and (1-v)), RoCoF constraints are violated for DUT 1&2 and DUT 4 (violation of condition (1-vii)), and pronounced oscillations appear for SG-based DUTs 5-7 (violation of condition (1-viii)). Overall, these results demonstrate that the proposed NGGC conditions capture key stability and performance trends and provide meaningful guidance for device-level control design.

VI. CONCLUSION

This paper presented preliminary results toward a decentralized, frequency-domain framework for certifying stability and performance in *Next Generation Grid Codes*. The approach provides an initial, model-agnostic basis for linking local device behavior to system-level stability and performance. Ongoing work is extending these findings through larger-scale numerical studies with detailed network and device models, which will also investigate the dynamic behavior of the qv-subsystem.

	(1-i)	(1-ii)	(1-iii)	(1-iv)	(1-v)	(1-vi)	(1-vii)	(1-viii)
DUT 1 & 2	✗	✓	✓	✗	✓	✓	✗	✓
DUT 3	✓	✓	✓	✓	✓	✓	✓	✓
DUT 4	✓	✓	✓	✗	✓	✓	✗	✓
DUT 5	✓	✗	✗	✓	✗	✓	✓	✗
DUT 6	✓	✓	✗	✓	✗	✓	✓	✗
DUT 7	✓	✗	✗	✓	✗	✓	✓	✗

TABLE I: NGGC compliance of the different DUT control laws $D_2^pf(s)$.

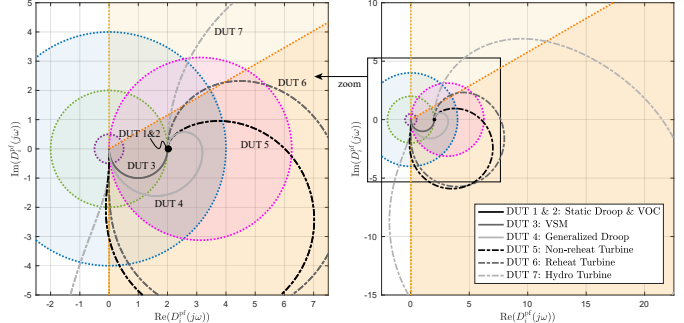
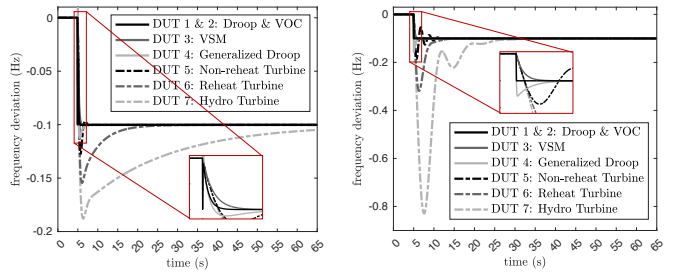


Fig. 6: Nyquist plots of the DUT controllers $D_2^pf(s)$, with NGGC conditions indicated using the same colors as in Fig. 5.



(a) First experiment. (b) Second experiment.

Fig. 7: Average-mode frequency responses of the two-node test system.

REFERENCES

- [1] “Commission regulation (EU) 2016/631 of 14 april 2016, establishing a network code on requirements for grid connection of generators,” tech. rep., European Commission, 2016.
- [2] “The technical requirements and the prequalification process of fast frequency reserve (ffr),” tech. rep., Oyj, Fingrid, 2021.
- [3] “Techn. Anforderungen an Netzbildende Eigenschaften inkl. der Bereitstellung von Momentanreserve,” tech. rep., VDE FNN Hinweis, 2024.
- [4] D. Groß, “Compensating network dynamics in grid-forming control,” in *58th Annual Allerton Conference on Communication, Control, and Computing (Allerton)*, 2022.
- [5] H. Geng, X. Xi, and G. Yang, “Small-signal stability of power system integrated with ancillary-controlled large-scale DFIG-based wind farm,” *IET Renewable Power Generation*, vol. 11, no. 8, pp. 1191–1198, 2017.
- [6] “Technical requirements for frequency containment reserve provision in the nordic synchronous area,” tech. rep., ENTSO-E, 2022.
- [7] A. Hoke *et al.*, “White paper: Grid forming functional specifications for bps-connected battery energy storage systems,” tech. rep., North American Electric Reliability Corporation (NERC), 2023.
- [8] Z. Siahaan, E. Mallada, and S. Geng, “Decentralized stability criteria for grid-forming control in inverter-based power systems,” in *IEEE Power & Energy Society General Meeting*, 2024.
- [9] V. Häberle, X. He, L. Huang, F. Dörfler, and S. Low, “Decentralized parametric stability certificates for grid-forming converter control,” *arXiv preprint arXiv:2503.05403*, 2025.
- [10] L. Huang, D. Wang, X. Wang, H. Xin, P. Ju, K. H. Johansson, and F. Dörfler, “Gain and phase: Decentralized stability conditions for power electronics-dominated power systems,” *IEEE Transactions on Power Systems*, vol. 39, no. 6, pp. 7240–7256, 2024.
- [11] L. Huang, L. Luo, R. Leng, H. Xin, D. Wang, and F. Dörfler, “Geometric decentralized stability condition for power systems based on projecting dw shells,” *arXiv:2508.17033*, 2025.
- [12] Y. Jiang, A. Bernstein, P. Vorobev, and E. Mallada, “Grid-forming frequency shaping control for low-inertia power systems,” in *2021 American Control Conference (ACC)*, pp. 4184–4189, 2021.
- [13] A. Papoulis, *The Fourier Integral and its Applications*. McGraw-Hill, New York, 1962.
- [14] P. Kundur, *Power System Stability and Control*. McGraw-Hill, 1994.